A robust workflow for performing joint impedance inversion with applications from North American Basins

Ritesh Kumar Sharma[†*]*, Satinder Chopra*[†] *and Larry R. Lines*[+]
[†]*TGS, Calgary;* [+] *University of Calgary, Canada*

Summary

Multicomponent seismic data offers many advantages for characterizing reservoirs with the use of the vertical component (PP) and the mode-converted (PS) data. Joint impedance inversion inverts both these datasets simultaneously, and hence is considered superior to simultaneous impedance inversion. However, the success of joint impedance inversion depends on how accurately the PS data is mapped on the PP time domain. Normally, this is attempted by following well-to-seismic ties for both PP and PS datasets, and the matching of different horizons picked on both PP and PS data. Though, it seems to be a straightforward approach there are a few issues associated with it. One of them is the lower resolution of the PS data than the PP data which presents difficulties in the correlation of the equivalent reflection events on both the datasets. Even if few consistent horizons get tracked, the horizon matching process introduces some artifacts on the PS data mapped into PP time. In this exercise, we elaborate on such challenges with a dataset from the Western Canadian Sedimentary Basin and then propose a novel workflow for addressing them. The value addition provided by the proposed workflow has been demonstrated by comparing data examples generated both with and without its adoption.

Introduction

Multicomponent seismic data offers many advantages for characterizing reservoirs with the use of the vertical component (PP) and the mode-converted (PS) data. These include imaging through gas clouds (Knapp et al., 2001; Nolte et al., 2000), lithology and fluid discrimination (Tatham and Krug, 1985; Macleod et al., 1999), fracture characterization (Kristiansen et al., 2005) amongst others. After processing of multicomponent seismic data, the outputs are PP-wave data processed in PP two-way time and PS-wave data processed in PS time scale. Even though the PS data is expected to add significant information to the conventional PP data interpretation, the difference in their time scales prevents an easy visual comparison between them while doing their joint interpretation. Converting PS data to PP two-way travel time would help accomplish this objective. Another motivation for going from PS to PP time is that many of the above-stated applications for multicomponent data are accomplished by putting the data through an integrated or joint impedance inversion. Any such inversion would expect both the datasets to be in the same two-way travel time, preferably PP time.

A consistent and joint interpretation of PP and PS data depends on the identification of reflections corresponding to similar geologic events on both datasets. This is accomplished by performing well-log correlations with PP and PS seismic data, i.e. PP data are correlated with PP synthetic seismogram in PP two-way travel time, and similarly PS data are correlated with PS synthetic seismogram in PS two-way travel time. It is assumed here that dipole sonic curves are available and both synthetic seismograms are generated over the same range of frequency bandwidth as the input reflection data. Such a correlation helps the seismic interpreter pick reflection events on PS data that occur at the same stratigraphic boundary on PP data.

Once the equivalent correlative events on the PP and PS data volumes are tracked, they are used to map or shrink the PS time scale to the PP time scale, a process referred to as *registration*. This step may not be straightforward as a peak on the PP data may not necessarily correspond to a peak on the PS data. In the case of complex geology entailing faulting, horizons may be difficult to interpret. Added to this difficulty is the fact that the frequency content of PP and PS data are different, as component frequencies are attenuated differently during wave propagation. The PP data typically exhibit higher frequencies than the PS data. Thus, the lower resolution of the PS data than the PP data also presents difficulties in the correlation of the equivalent reflection events. Even though some automated methods have been introduced for registration of PS to PP times, in the absence of such methods, the above-mentioned manual registration exercise is usually performed. As this is a crucial step before going forward to performing joint impedance inversion, it needs to be done carefully, or else it can result in artifacts on the impedance data. We elaborate on some of these challenges as applicable to a dataset from the WCSB and present a new workflow for addressing them.

Artifacts with conventional workflow

In Figure 1, we show the well-to-seismic correlation for PS data. The well-log curves are shown in Figure 1a, and the PS synthetic seismogram (blue traces) correlation with real PS seismic data (red traces) is seen in Figure 1b. The correlation between the two was found to be 93%, which is very encouraging. A segment of the PS data in PS time is shown in Figure 1c. Horizon picking is now carried out to map all the trackable horizons on PS data as shown in magenta. Once the well-to-seismic correlation for PP and PS data are done satisfactorily, the depth-time curves for both are determined and used for estimation of V_P/V_S. Next, the determined interval V_P/V_S at the well is propagated over the 3D seismic data to obtain an initial V_P/V_S volume, which is used to transform PS data from its original time domain to PP time domain. Had it been valid everywhere, a perfect match between PP and PS horizons would have been noticed. However, a mismatch (except at the location of well used in the correlation) between these two types of horizons is

10.1190/segam2019-3214092.1

usually seen as shown in Figure 2a and b. Geologically, such a mismatch is not acceptable, as a geological marker would be expected at the same time on both the datasets after conversion of PS time into PP, or vice versa. It happens because the interval V_P/V_S function is valid at the location of the well only and may not be valid at other lateral locations. For ensuring that the horizons on both PP and PS data are geologically consistent, we try and match the picked horizons (blue and magenta) on both datasets. The discrepancies in the V_P/V_S used in the domain conversion can be estimated on comparing it with V_P/V_S computed using equation (Lines et al., 2005) below.

$$\frac{V_P}{V_S} = 2\left(\frac{PS\ isochron}{PP\ isochron}\right) - 1. \quad (1)$$

The V_P/V_S values so computed at every trace are compared with the initial V_P/V_S volume. The observed differences in V_P/V_S are then spread out within the individual intervals at every CDP location, resulting in time shifts of reflection events. While this process tends to solve the mismatch problem at the boundaries of various intervals bounded by horizons, it creates some artifacts within the intervals as shown in Figure 2c, where an equivalent segment of PS section in PP time (Figure 2b) is shown after horizon matching. The overlay in color is the V_P/V_S. The revised values are again shown in color but are abnormal in the lower part of the section. The distorted reflections in the form of undulations in the middle of the sections are also not acceptable. Such artifacts if not corrected before performing joint inversion could degrade the results. We show this in Figure 3, where a section from the PP data is shown (Figure 3a), along with its equivalent section from PS data in PP time (Figure 3b). Notice the artifacts seen as jitter in the reflections on the left side of the PS section in Figure 3b, as well as the distinctly different character indicated in dashed black outline. Such artifacts should be corrected for before joint inversion is performed, or else they could get accentuated as shown in Figure 4.

The other issue mentioned above is about the spectral bandwidth difference between the PP and PS data in PP time. This is found to be the case almost always, and results in degradation of the joint impedance inversion performance. In Figure 5a we show a frequency spectra comparison of the wavelets extracted from both the PP and PS data in PP time. Notice the large difference in their frequency content.

Addressing the artifacts

Figure 6 shows a block diagram for the proposed workflow that may be adopted to address the above-mentioned artifacts.

To begin with, we transform PS data into PP time using horizons that bound the broad zone of interest. Then we flatten the frequency spectra of this data by balancing the power, which is simply the square of the spectral magnitude. Such an approach was first discussed by Marfurt and Matos (2014) and makes use of the average power spectrum at a given time as well as the average spectral magnitude. As a single time-varying spectral balancing operator is applied to every trace, this spectral balancing approach is considered amplitude friendly (Chopra and Marfurt, 2016). In Figure 5b we show the equivalent frequency spectra and the wavelets for the PP and PS spectrally-balanced data in PP time. Notice the flattened frequency spectra of the PS data now. The next step is to normalize the PP and the spectrally-balanced PS data using z-transformation. Thereafter, using the picked horizons, stratal intervals are defined over the broad zone of interest. The individual stratal units on the PP and PS data are crosscorrelated to find the time shifts for maximum correlation, and by linear interpolation a volume of time shifts is generated that would align the PP and PS data.

In Figure 7 we show the PS section after the application of the proposed workflow, equivalent to the one shown in Figure 3b. Notice the drastic reduction of the jitter on the left side of the section, as well as the much better definition of the reflection event enclosed in black dashed outline. The overall quality of the section exhibits an uplift, which is not just visual. The data were carried forward to joint impedance inversion and both the resultant products, P- as well as S-impedance data were examined. Notice the much better correlation of the P-impedance with the overlaid impedance log strips on the arbitrary line in Figure 8, as compared with the equivalent display shown in Figure 4.

Finally, in Figure 9, we show stratal slice comparisons between the conventional approach and our proposed approach, from the P-impedance and the V_P/V_S volumes obtained from joint impedance inversion. We believe the results are convincing which would result in more accurate interpretation, and thus drilling outcomes.

Conclusions

We have drawn attention to a couple of relevant issues that are often seen in the conventional approach followed for registration of multicomponent PP and PS seismic data. If such issues are not addressed, they can lead to artifacts in the joint impedance inversion carried out for generation of elastic parameters. Our suggested workflow addresses the discussed issues and produces results that are far superior to those obtained with conventional workflows.

Acknowledgements

We wish to thank TGS for encouraging this work and for the permission to present and publish it. The well data used in this work was obtained from the TGS Well Data Library and is gratefully acknowledged.

10.1190/segam2019-3214092.1

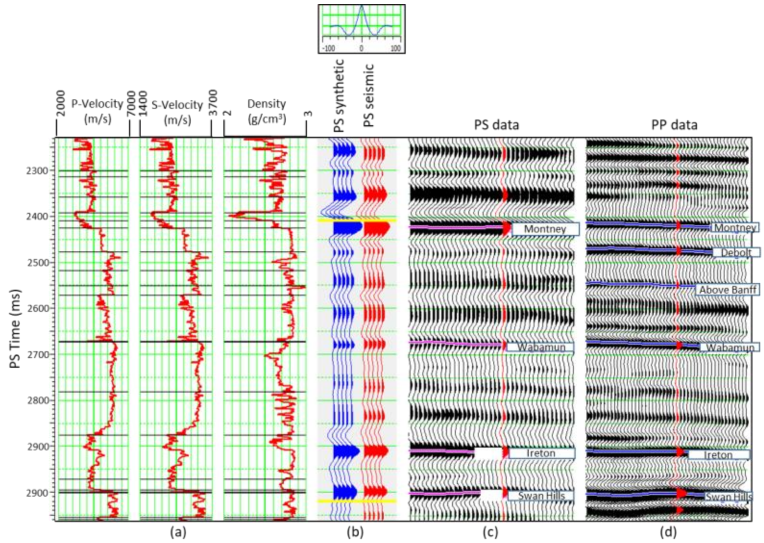

Figure 1. Well-to-seismic correlation for PS data as well as registration with PP data, at the location of a well. The PS synthetic seismogram (blue traces) is shown in (b) correlated with PS real seismic traces (in red). The displayed wavelet, used for generation of the synthetic seismogram, was extracted from the PS seismic data using a statistical process. The PS (c) and PP data (d) are shown in PS time (*Data courtesy of TGS, Calgary*).

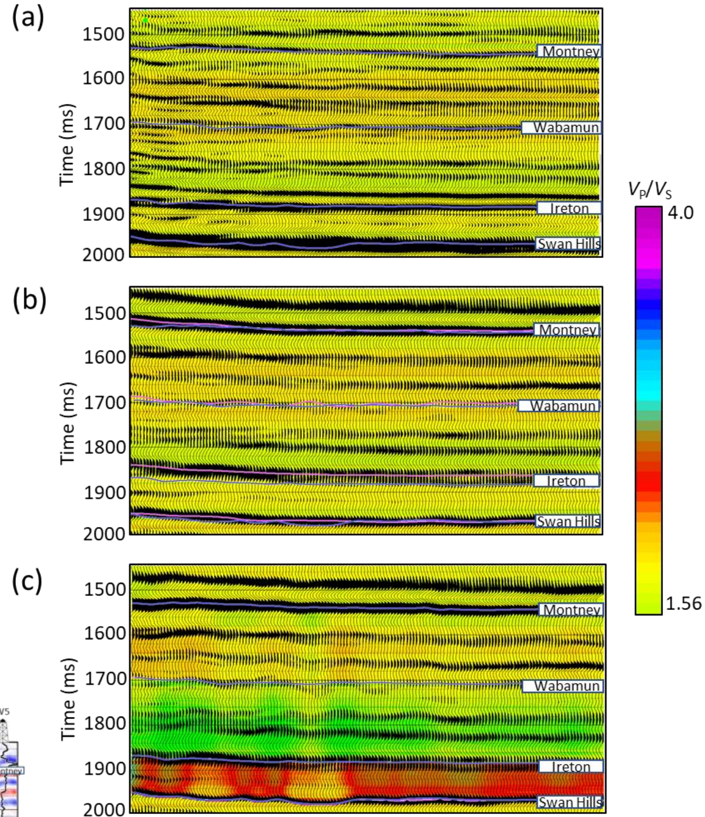

Figure 2. Segments of seismic sections from (a) PP and (b) PS data in PP time. Four equivalent reflection events have been picked on the data volumes separately as seen by the blue horizons picked on the PP data and the magenta horizons on the PS data, but the horizon matching has not been done yet. The V_P/V_S values at every CDP are overlaid in color. (c) The same PS section as in (b) but with the horizons (blue and magenta) matched. Notice, the revised values of V_P/V_S (which seem abnormal in the lower intervals) as well as the reflection distortions in the form of undulations. (*Data courtesy of TGS, Calgary*).

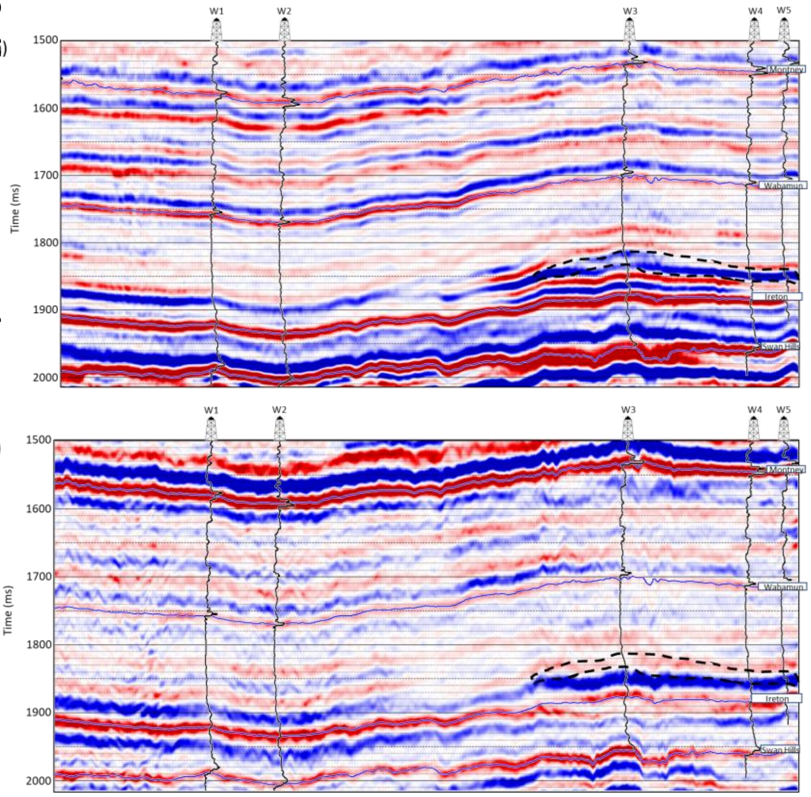

Figure 3. An arbitrary line section from (a) PP and (b) PS data in PP time after horizon matching. Four horizons have been picked on the sections and the impedance log curves have been overlaid. Notice in (b) there is some jitter seen on the left part, which is concerning. Also, the segment of the reflection event depicted in dashed black outline has a distinctly different character on the PS section, which prevents the imaging to this event on the impedance section. Both these observations signify artifacts. (*Data courtesy of TGS, Calgary*).

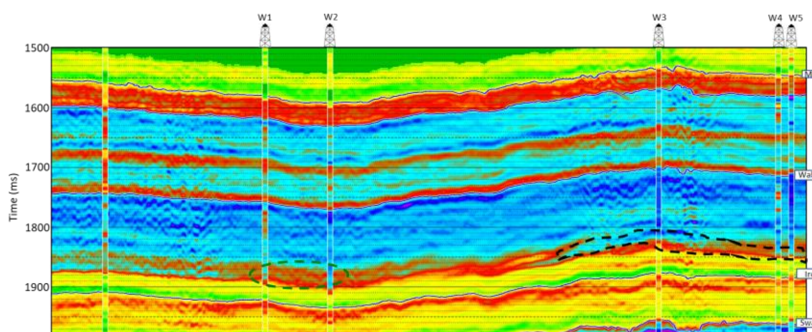

Figure 4. An arbitrary line section from the P-impedance volume with four horizons and impedance log curves overlaid. Apparently, the inversion has not performed optimally. Notice the jitter on the left side of the section as well as the reflection event in black dashed outline in Figure 3 carried through in the inversion. The mismatch between the inverted impedance and that measured in wells W1 and W2 (dark green dashed outline) as well as W4 and W5 can be seen clearly. (*Data courtesy of TGS, Calgary*).

10.1190/segam2019-3214092.1

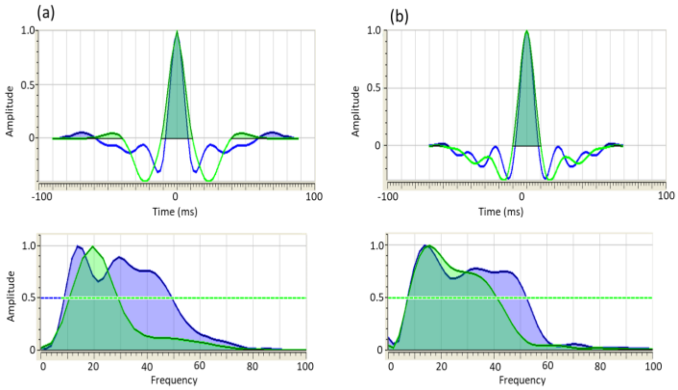

Figure 5: Wavelets and their frequency spectra extracted from PP and PS data in PP time (a) before and (b) after spectral balancing. The frequency content of PS data is appreciably lower than the PP data before balancing is significantly improved.

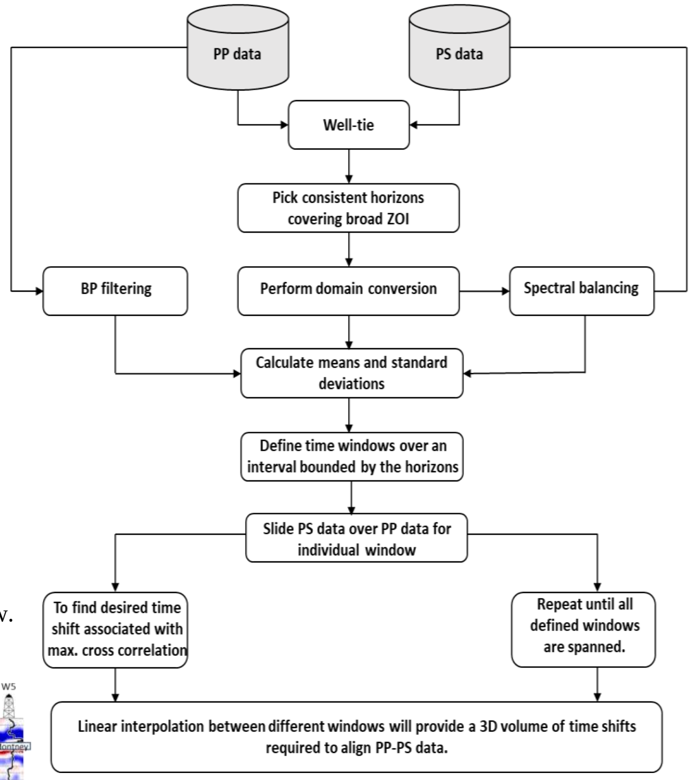

Figure 6: Block diagram explaining the proposed workflow.

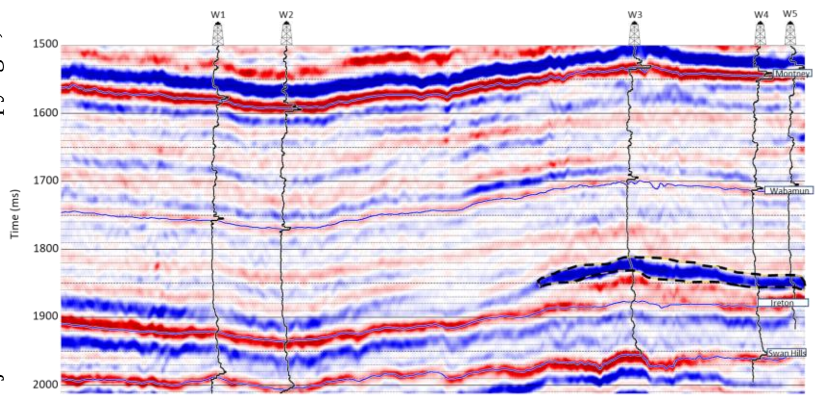

Figure 7. An arbitrary line section from PS data in PP time after spectral balancing and horizon matching. Which is equivalent to the similar section shown in Figure 3b. Notice the much better quality of this section and without artifacts. (*Data courtesy of TGS, Calgary*).

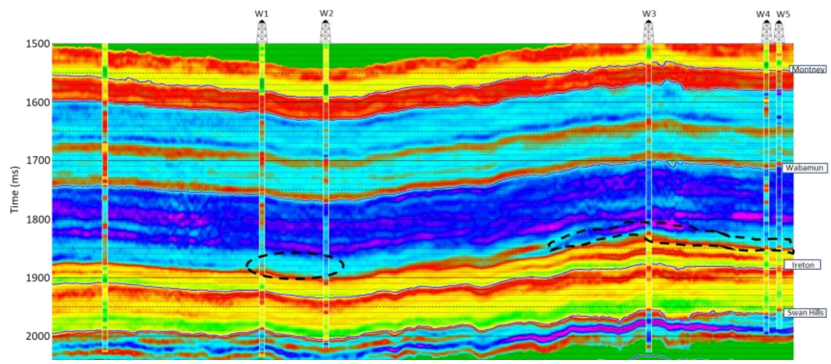

Figure 8. An arbitrary line section from the P-impedance volume generated using the proposed workflow, with four horizons and impedance log curves overlaid, which is equivalent to the section shown in Figure 4. The section shows much better correlation with the overlaid P-impedance log curves, and is free of artifacts. (*Data courtesy of TGS, Calgary*).

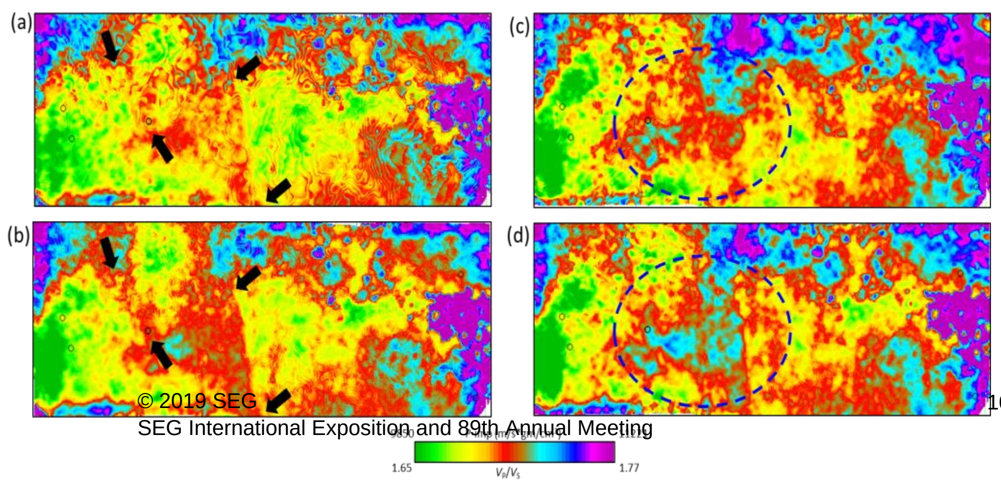

Figure 9. Comparison of stratal slices averaged over a 20 ms time window above the Swan Hills marker from the P-impedance volume generated using the (a) conventional workflow, and (b) the proposed workflow. Equivalent stratal slices extracted from the V_P/V_S volume are shown in (c) and (d). Notice the much better spatial resolution on the displays obtained after the proposed workflow as is pointed by the black block arrows on the left and in the region highlighted by the dashed circles. (*Data courtesy of TGS, Calgary*).

REFERENCES

Chopra, S., and K. J. Marfurt, 2016, Spectral decomposition and spectral balancing of seismic data: The Leading Edge, **35**, 176–179, doi: https://doi.org/10.1190/tle35020176.1.

Knapp, S., N. Payne, and T. Johns, 2001, Imaging through gas clouds: A case history from the Gulf of Mexico: 71st Annual International Meeting, SEG, Expanded Abstracts, 776–779, doi: https://doi.org/10.1190/1.1816747.

Kristiansen, P., J. Gaiser, and T. Probert, 2005, Fracture characterization using multicomponent surface seismic data: IPTC 10842, 1–6.

Lines, L. R., Y. Zou, D. A. Zhang, K. Hall, J. Embleton, B. Palmiere, C. Reine, P. Bessette, P. Cary, and D. Secord, 2005, VP/VS characterization of a heavy-oil reservoir: The Leading Edge, **24**, 1134–1136.

Macleod, M. K., R. A. Hanson, and S. McHugo, 1999, The Alba Field ocean bottom cable seismic survey: Impact on development: The Leading Edge, **18**, 1306–1312, doi: https://doi.org/10.1190/1.1438206.

Marfurt, K., and M. Matos, 2014, Am I blue? Finding the right (spectral) balance: AAPG Explorer, https://doi.org/http://www.aapg.org/ publications/news/explorer/column/article id/9522/am-i-blue- finding-the-right-spectral-balance, accessed 12 March 2015.

Nolte, B., D. Sukup, P. Krail, B. Temple, and B. Cafarelli, 2000, Anisotropic 3D prestack depth imaging of the Donald Field with converted waves: 70th Annual International Meeting, SEG, Expanded Abstracts, 1158, doi: https://doi.org/10.1190/1.1815595.

Tatham, R. H., and E. H. Krug, 1985, VP/VS Interpretation, *in* A. A. Fitch, ed., Developments in geophysical exploration methods: Elsevier Applied Science Publishers, 264, 139–188.

Chopra, S., and K. J., Marfurt, 2016, Spectral decomposition and spectral balancing of seismic data: The Leading Edge, **35**, 176–179, doi: https://doi.org/10.1190/tle35020176.1.

Knapp, S., N., Payne, and T., Johns, 2001, Imaging through gas clouds: A case history from the Gulf of Mexico: 71st Annual International Meeting, SEG, Expanded Abstracts, 776–779, doi: https://doi.org/10.1190/1.1816747.

Kristiansen, P., J., Gaiser, and T., Probert, 2005, Fracture characterization using multicomponent surface seismic data: IPTC 10842, 1–6.

Lines, L. R., Y., Zou, D. A., Zhang, K., Hall, J., Embleton, B., Palmiere, C., Reine, P., Bessette, P., Cary, and D., Secord, 2005, VP/VS characterization of a heavy-oil reservoir: The Leading Edge, **24**, 1134–1136.

Macleod, M. K., R. A., Hanson, and S., McHugo, 1999, The Alba Field ocean bottom cable seismic survey: Impact on development: The Leading Edge, **18**, 1306–1312, doi: https://doi.org/10.1190/1.1438206.

Marfurt, K., and M., Matos, 2014, Am I blue? Finding the right (spectral) balance: AAPG Explorer, http://www.aapg.org/ publications/news/explorer/column/article id/9522/am-i-blue- finding-the-right-spectral-balance, accessed 12 March 2015.

Nolte, B., D., Sukup, P., Krail, B., Temple, and B., Cafarelli, 2000, Anisotropic 3D prestack depth imaging of the Donald Field with converted waves: 70th Annual International Meeting, SEG, Expanded Abstracts, 1158, doi: https://doi.org/10.1190/1.1815595.

Tatham, R. H., and E. H., Krug, 1985, VP/VS Interpretation, *in* A. A. Fitch, ed., Developments in geophysical exploration methods: Elsevier Applied Science Publishers, 264, 139–188.

10.1190/segam2019-3214092.1